Available online at www.sciencedirect.com
ScienceDirect
Ceramics International 36 (2010) 1659–1667
CERAMICS INTERNATIONAL
www.elsevier.com/locate/ceramint

Fabrication and characterization of sol–gel derived hydroxyapatite/zirconia composite nanopowders with various yttria contents

S. Salehi *, M.H. Fathi

Biomaterials Group, Department of Materials Engineering, Isfahan University of Technology, Isfahan 84156-83111, Iran

Received 17 November 2009; received in revised form 18 December 2009; accepted 26 February 2010
Available online 24 April 2010

Abstract

Homogeneous composite nanopowders of hydroxyapatite/30 wt% yttria-stabilized zirconia (HA–YSZ) containing 0, 3, 5, and 8 mol% Y_2O_3 (namely; HA–0YSZ, HA–3YSZ, HA–5YSZ, and HA–8YSZ) were successfully synthesized using the sol–gel method. Simultaneous thermal analysis (STA), X-ray diffraction (XRD), X-ray fluorescence spectroscopy (XRF), Fourier transformed infrared (FTIR) spectroscopy, scanning electron microscopy (SEM), and transmission electron microscopy (TEM) techniques were utilized to characterize the prepared nanopowders. Analyses of HA–YSZ composite nanopowders showed the successful formation of desirable phases. HA unit cell volume in the composites increased as a result of ion exchange of calcium and zirconium between HA and zirconia. Results revealed the formation of HA particles with irregular morphology (40–80 nm) and spherical yttria-stabilized zirconia particles (20–30 nm). Segregation of yttrium ions at the grain boundaries of ZrO_2 particles retarded the grain growth of zirconia particles and the presence of ZrO_2 nanoparticles among the hydroxyapatite particles resulted in grain growth inhibition of HA particles. This process can be used to synthesize HA–YSZ composite nanopowders with improved properties, which are much needed for hard tissue repair and biomedical applications.

Keywords: A. Sol–gel processes; B. Nanocomposites; C. ZrO_2; D. Biomedical applications

1. Introduction

Hydroxyapatite [HA, $Ca_{10}(PO_4)_6(OH)_2$], a major inorganic component of the bone, has been used extensively in biomedical applications and bone regeneration due to its biodegradable, bioactive, and osteoconductive properties [1,2]. However, usage of pure HA is limited on account of the principal limitation of this material ''weakness and brittleness'', which restricts its clinical orthopedic and load-bearing applications [3].

A well-known method for improvement of the inherent mechanical properties of HA is based on the synthesis of composites consisted of HA and other reinforcement phases. This approach has taken much attention since the successful development of ceramic–matrix composite (CMC) materials [2,3].

An effective reinforcing agent for a CMC material acts under specific conditions. First, the strength of the reinforcing phase must be higher than that of the matrix. Second, the interfacial strength between the matrix and the reinforcing phase should be neither too weak nor too strong. In the case of biomaterials, the biocompatibility of the second phase is another important factor that should be considered [4].

For HA reinforcement, ceramics such as zirconia (ZrO_2) which have already been used in load-bearing biomedical applications, can also be suggested on account of higher strength and fracture toughness of ZrO_2 [5]. As shown previously by Miao et al. [5], HA–ZrO_2 composites exhibit significantly higher mechanical properties (bending strength, microhardness, and Young's modulus) than those of pure HA.

Partially stabilized zirconia (PSZ) can be obtained in such system as ZrO_2–Y_2O_3, ZrO_2–CaO. In these systems, it is possible to obtain ceramics formed at room temperature with a tetragonal or cubic phase or tetragonal-cubic phases [6]. The crystal structure of yttria-stabilized zirconia (YSZ) varies from a monoclinic and tetragonal multiphase to a cubic symmetry with the increase of Y_2O_3 content from 3 mol% up to 8 mol% [7].

* Corresponding author. Tel.: +98 913 408 6820; fax: +98 311 391 2752.
E-mail address: salehi@ma.iut.ac.ir (S. Salehi).

0272-8842/$36.00
doi:10.1016/j.ceramint.2010.02.045

Mutual reaction between YSZ and HA seems avoidable. The presence of zirconia decreases the decomposition temperature of HA. The decomposition of HA results in changes in the physical and chemical properties of the material and thus affects the performance of implant material in a living body [8]. HA decomposition is, therefore, an important problem both from a scientific and a biomedical application viewpoint.

In order to obtain a HA–YSZ composite with fine grains, it is necessary to prepare nanoparticles with a low sintering temperature. In addition, nanostructured HA is expected to have superior mechanical properties in comparison with conventional HA used in implant systems. Also, the presence of the grains of the nanometer-size and high volume fractions of grain boundaries in HA has been found to increase osteoblast adhesion, proliferation, and mineralization [2,9,10].

Various methods have been reported for the synthesis of HA–YSZ nanopowders, such as co-precipitation [11] and solid state reaction [12]. However, these methods have some disadvantages such as difficulty of control and high costs. Recently, the sol–gel process has been widely used in the manufacturing of ceramics because of its intrinsic advantages over other conventional processes [13]. The sol–gel process is a wet chemical method that does not depend on high pH values or high sintering temperatures. The high surface area of dried gels results in high reactivity which permits a low process temperature. Moreover, the method offers a molecular mixing precursor solution which is capable of improving chemical homogeneity [13]. Finally, the process allows the preparation of a homogeneous mixture of HA and YSZ nanoparticles.

The aim of the present study was to prepare HA–YSZ composite nanopowders directly through the sol–gel method beside the determination of chemical and physical properties of the resulting composite at the optimum calcination temperature. Also, the effect of yttria content on the microstructure of the sol–gel derived HA–YSZ composite nanopowders was investigated.

2. Experimental

2.1. Preparation of composite nanopowders

An experimental procedure similar to that described by Liu et al. [14] was followed for the synthesis of the hydroxyapatite sol. Briefly, a phosphite sol was prepared by hydrolysing triethyl phosphite ($(C_2H_5O)_3P$, Fluka) for 24 h with a fixed amount of distilled water and ethanol absolute (the molar ratio of water and ethanol to phosphite were fixed at 4) in a sealed glass container under vigorous stirring at room temperature. A stoichiometric amount of calcium nitrate tetrahydrate ($Ca(NO_3)_2{\cdot}4H_2O$, Merck) dissolved in ethanol absolute was added dropwise into the hydrolyzed phosphite sol. The concentration of the calcium and phosphorus solution was kept constant to maintain the stoichiometry of HA (~1.67). Vigorous stirring was continued for an additional 24 h after titration. Zirconium isopropoxide isopropanol complex ($Zr(O\text{-}C_3H_7)_4OC_3H_8$, Aldrich) diluted in 2-propanol (Merck) was used as the source of zirconia. Yttrium (III) acetate hydrate ($(CH_3CO_2)_3Y{\cdot}xH_2O$, Sigma) and glacial acetic acid (AcH) were used as stabilizing agents. The first step in the formation of zirconia sol is to obtain a stable sol, which consists of zirconia sol and yttrium acetate. Firstly, zirconia sol was prepared and then mixed with yttrium acetate. Glacial acetic acid was dripped into the zirconia sol to form a complex compound by the reaction of AcH with $Zr(OC_3H_7)_4OC_3H_8$. The greater reactivity of $Zr(OC_3H_7)_4OC_3H_8$ demands strict control over the hydrolysis conditions in order to prepare a homogeneous sol rather than a precipitate. As the hydrolysis reaction can take place even in an atmosphere of low humidity, hydrolysis conditions were strictly controlled. Thus, the glass containers used to contain the solutions were covered with plastic wraps to inhibit evaporation. The yttria precursor was obtained by solubilization of 0, 3, 5, and 8 mol% yttrium acetate in 2-propanol. After the addition of yttrium acetate to the zirconia sol, distilled water was dripped into the mixed solution. The source solution was homogenized with stabilizing agents under vigorous stirring for 24 h. No catalytic agent was used in this work and the mixed solution was prepared at room temperatures of 20–25 °C. The molar ratios of water to Zr, 2-propanol to Zr, and acetic acid to Zr were set at 10:1, 50:1, and 5:1, respectively. The reinforcements were prepared by 30 wt% ZrO_2 sol concentration. Finally, a mixture of the zirconia sol and the hydroxyapatite sol was used to synthesize HA–YSZ composites. Fortunately, no gelation was observed despite the addition and a stable HA–YSZ composite sol was achieved. The reinforcement solutions were constantly stirred for 24 h followed by 4 h of aging. After aging, the obtained gels were oven dried at 80 °C and calcined at 850, 950, and 1050 °C for 1 h to get crystalline powders. Therefore, four different types of zirconia, namely pure, 3 mol%, 5 mol%, and 8 mol% yttria doped, were used to make the HA–YSZ composite powders specimens.

2.2. Composite powder characterization

The thermal behavior of the composite dried gels was investigated using a TG/DTA analyzer (Germany, Linseis, L70/2171). The thermogravimetric analysis (TG) and the differential thermal analysis (DTA) of the composite dried gels during heating were recorded from 20 to 1200 °C at a heating rate of 10 °C/min in the air.

Phase characterization of HA–YSZ composite nanopowders was performed using the X-ray diffractometer (XRD) (Philips X'Pert-MPD, Cu Kα radiation: $\lambda = 0.154$ nm at 30 mA and 40 kV, over the 2θ range of 20–80° at a scan rate of 0.008°/min). The experimental patterns obtained were compared with the standards compiled by the Joint Committee on Powder Diffraction and Standards (JCPDS), which included card #09-432 [15] for HA, #17-0923 [16] for tetragonal (t)-ZrO_2, and #27-0997 [17] for cubic (c)-ZrO_2, respectively.

The grain sizes of the composite nanopowders were determined using broadening of XRD pattern peaks and Scherer's equation (Eq. (1)) [18].

$$D = \frac{0.89\lambda}{B\cos\theta} \quad (1)$$

where D is grain size (nm), λ is the wavelength of the X-ray beam, B is the width of the peak in the middle of its height, and θ is Bragg's angle (degree). The crystallinity of HA was estimated from the XRD data using Eq. (2) [19]:

$$Xc = 1 - \left(\frac{V_{112/300}}{I_{300}}\right) \quad (2)$$

in which, Xc is the degree of HA crystallinity, I_{300} is the intensity of the (3 0 0) peak, and $V_{1\,1\,2/3\,0\,0}$ is the intensity of the shoulder between the (1 1 2) and (3 0 0) diffraction peaks.

Lattice parameters of the HA included in composite powders were calculated using the standard relationships between the interplanar spacing ($d_{h\,k\,l}$) and the lattice parameters (a and c) for hexagonal systems [18]. The HA unit cell volume was calculated using the formula $V = 2.589a^2c$ [20].

The lattice parameter change in ZrO_2 was investigated using XRD data. The peak positions (2θ) of t-ZrO_2 (1 1 1), (2 2 0), and c-ZrO_2 (1 1 1) were precisely measured and inserted into Bragg's law and the interplanar d-spacing [18].

Weight percentages of zirconia, yttria, and Ca/P weight ratio in the HA–YSZ composite powders were measured by X-ray fluorescence spectroscopy (XRF, Bruker S4 PIONEER).

The functional groups of composite powders were analyzed with Fourier transformed infrared (FTIR) spectroscopy (Bomem, MB100). The spectra were recorded from 4000 to 400 cm^{-1} wave number with a resolution of 2 cm^{-1}.

A scanning electron microscope (SEM: Philips XL30) and a transmission electron microscope (TEM: Philips CM200) were utilized to evaluate the morphology and particle size of the synthesized HA–YSZ composite nanopowders.

3. Results and discussion

3.1. Characterization of mixed HA–YSZ sol

For the first time, we studied the effects of precursors to determine optimum conditions in the formation of HA–YSZ composites prepared by the sol–gel method. A reaction of AcH and $Zr(OC_3H_7)_4OC_3H_8$ is believed to prevent sol precipitation or gelation. When no AcH was added, a white precipitate was observed as a result of hydrolysis. The precipitate is considered as the molecular aggregate of hydrated zirconium oxide alkoxides ($Zr(OC_3H_7)_4OC_3H_8$), which is caused by the fast hydrolysis process. A molar ratio of AcH to Zr equal to 5:1, however, can stabilize $Zr(OC_3H_7)_4OC_3H_8$ and, thus, prevent immediate precipitation. Similar results were observed by Changrong et al. [21] in which zirconium alkoxide (zirconium tetra-n-propoxide) was found to be stabilized by AcH during the preparation of pure zirconia sols. Unfortunately, no further data was reported on details of the process.

Yttrium acetate reacts with zirconium alkoxides to form derivatives with the liberation of alkyl acetate. The reaction

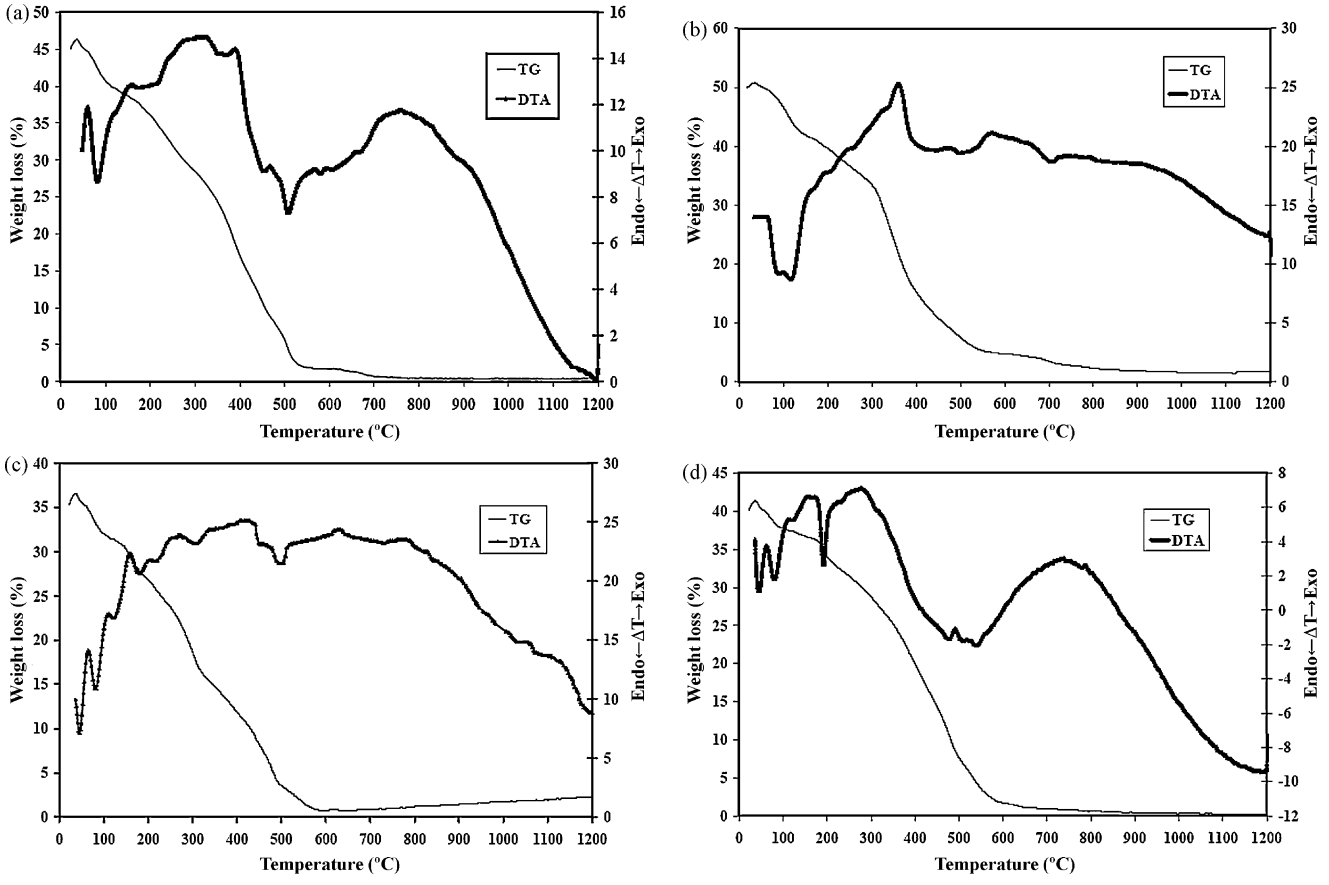

Fig. 1. Typical TG and DTA curves of (a) HA–0YAZ, (b) HA–3YSZ, (c) HA–5YSZ, and (d) HA–8YSZ composite dried gels from room temperature to 1200 °C.

then continues with further reaction of acetate and alkoxide group to increase molecular weight [22].

3.2. Thermal analysis of the dried gel

It is well specified that temperature control during the synthesis is crucial to influence the reaction progress and the properties of the HA–YSZ composite [11,12]. Thus, the thermal decomposition mechanism of the composite dried gels was studied by TG/DTA measurements. Additionally, the results of thermal decomposition of the dried gels were used for the determination of the optimum conditions for final calcination of the composite dried gels to obtain the desired biomaterial.

Fig. 1(a–d) shows the (TG/DTA) curves of the HA–YSZ composite dried gels measured at a heating rate of 10 °C/min. The total weight losses observed were about 45%, 44%, 35%, and 40% for HA–0YAZ, HA–3YSZ, HA–5YSZ, and HA–8YSZ dried gels, respectively, in the temperatures range of 25–1200 °C. No significant differences were observed in the thermal behavior of the composite dried gels. The severe weight losses at about 100–300 °C correspond to the evaporation of volatile component such as H_2O and combustion of organic components such as ethanol, and 2-propanol for the composite dried gels (Fig. 1(a–d)). An exothermic peak was observed at about 400 °C for the dried gel is attributed to the onset of crystalline apatite formation from the amorphous phase based on the XRD patterns [23,24]. The weak exothermic peak at 400–500 °C is due to the formation of the zirconia phase. This exothermic reaction is resulted from crystallization of the tetragonal structure of zirconia in the HA–3YSZ sample [25]. In addition, according to Kuo et al. [26,7], when the exothermic peak temperature is greater than 456 °C, only pure cubic ZrO_2 is obtained for 8YSZ.

3.3. XRD phase analysis

XRD patterns of the HA–YSZ composite powders obtained at the various calcination temperatures of 850 °C, 950 °C, and 1050 °C for 1 h are shown in Fig. 2 through 4, respectively. The composite powders calcined at 850 °C (Fig. 2) exhibit broad peaks, as a result of presence of poorly crystalline phases. From the powder diffraction patterns, the crystallinity of HA in each synthesized powder was calculated using Eq. (2) and the results were summarized in Table 1. Addition of zirconia caused more crystalline HA to transform into the amorphous calcium phosphate rather than decomposing into calcia (CaO) and β-TCP [27]. Thus, it was necessary to raise the calcination temperature. When the calcination temperature was raised to 950 °C, the hydroxyapatite and zirconia peaks became sharper and more apparent with increasing crystallinity (Fig. 3 and Table 1).

The effects of various amounts of Y_2O_3 on the phase transition of HA–YSZ composite powders are shown in Fig. 3. Peaks corresponding to zirconia phases are found in a tetragonal (t) structure in HA–3YSZ, a cubic (c) structure in HA–0YSZ and HA–8YSZ, and a dual phase (t–c) structure in HA–5YSZ composites. It has been reported that the addition of ZrO_2 to the HA matrix decreases the hydroxyapatite decomposition temperature, so that HA starts to decompose to a mixture of β-TCP and CaO according to the following reaction [28]:

$$Ca_{10}(PO_4)_6(OH)_2 = 3Ca_3(PO_4)_2 + CaO + H_2O$$

It has been proposed that HA decomposition is related to the transfer of CaO to the zirconia matrix, which results in the phase changes of HA and ZrO_2 [28]. Hence, the optimization of the calcination temperature is of great importance. Addition of a ZrO_2 phase such as 0YSZ to the HA matrix decreases the decomposition temperature of HA, so that HA starts to decompose into a mixture of TCP and CaO and that HA will react with the monoclinic (m)-ZrO_2 phase resulting in the formation of calcia-stabilized ZrO_2 according to the following reaction [29]:

$$Ca_{10}(PO_4)_6(OH)_2 + ZrO_2(m) = 3Ca_3(PO_4)_2 + \text{CaO-doped } ZrO_2 + H_2O$$

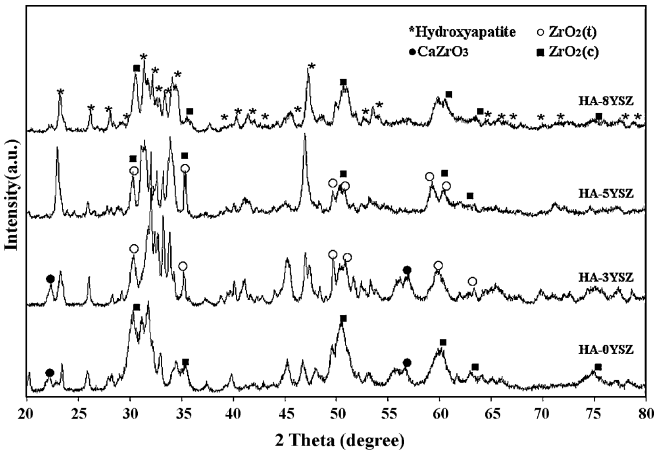

Fig. 2. XRD patterns of composite nanopowders obtained with various amounts of Y_2O_3 after calcination at temperature of 850 °C for 1 h.

Table 1
Calculated grain sizes and HA crystallinity of the prepared HA–YSZ composite nanopowders with various amounts of Y_2O_3 and calcination at different temperatures for 1 h.

Sample	*d* HA (nm)	*d* ZrO_2 (nm)	Crystallinity (%)
HA–0YSZ/850	32	19	46
HA–3YSZ/850	40	15	60
HA–5YSZ/850	48	8	61
HA–8YSZ/850	75	10	54
HA–0YSZ/950	61	31	61
HA–3YSZ/950	71	29	70
HA–5YSZ/950	65	26	68
HA–8YSZ/950	78	25	60
HA–0YSZ/1050	68	57	70
HA–3YSZ/1050	78	50	75
HA–5YSZ/1050	80	42	72
HA–8YSZ/1050	82	41	78

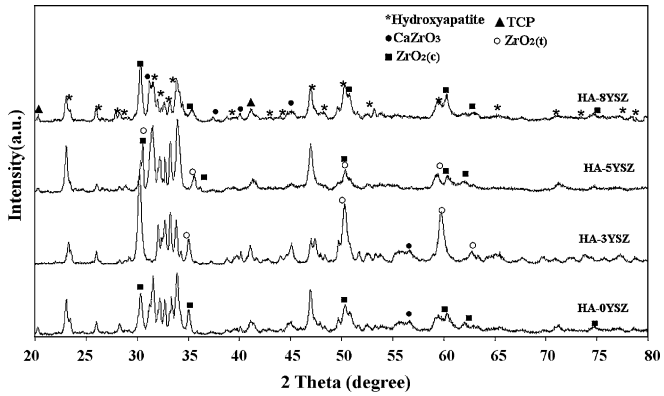

Fig. 3. XRD patterns of composite nanopowders obtained with various amounts of Y_2O_3 after calcination at temperature of 950 °C for 1 h.

This behavior is different from that of pure HA, so that ZrO_2 act as a catalyst for the decomposition of HA [29]. Some CaO will subsequently dissolve into zirconia to form a solid solution followed by a phase change from the tetragonal phase to the cubic phase with the formation of calcia-stabilized zirconia, as shown in the CaO–ZrO_2 [30] phase diagram.

This trend continues until a balance has been reached for calcium at both sides of the diffusion couple HA and ZrO_2 and identical chemical potentials of calcium ions are obtained in HA and ZrO_2. The other CaO will react with ZrO_2 to form calcium zirconate ($CaZrO_3$). Meanwhile, these reactions cause HA to become destabilized and decompose into more β-TCP phases [11,29]. On the other hand, as more CaO is available from HA decomposition, $CaZrO_3$ forms as in the following reaction. CaO concentration reaches saturation solubility throughout the ZrO_2 particles, so that any additional CaO should be consumed to form $CaZrO_3$ [30,31].

$$Ca_{10}(PO_4)_6(OH)_2 + \text{Ca-doped}\,ZrO_2(t) = Ca_3(PO_4)_2 + CaZrO_3$$

When zirconia is stabilized with Y_2O_3, it will be in tetragonal and cubic structures with no monoclinic ZrO_2 phase [6]. The phase transition of zirconia with various amounts of Y_2O_3 (mol%) was interpreted as the diffusion of Y_2O_3 ions into the zirconia crystals, a conclusion that was confirmed by the ZrO_2–Y_2O_3 phase diagram [6]. Therefore, the resulting powder is less reactive with CaO than the pure monoclinic ZrO_2 is. It has been reported that, the reason for this lower reactivity is that the diffusion of CaO in ZrO_2 containing some Y_2O_3 is slower than in ZrO_2 without it [29,31]. Thus, the effect of Y_2O_3 is apparently one of reducing the diffusion coefficient of CaO in ZrO_2 [31]. Some of the defects which play a great role in the diffusion are taken up by the Y_2O_3, leaving fewer defects for CaO diffusion. $CaZrO_3$ begins to form at lower temperatures with ZrO_2 containing Y_2O_3 than with composites of pure zirconia, probably because of the greater CaO build up at the ZrO_2 surface as a result of slower CaO diffusion in ZrO_2 [28]. The direct reaction between HA and YSZ was, therefore, assumed to be as in the following reaction [25]:

$$Ca_{10}(PO_4)_6(OH)_2 + \text{Y-}ZrO_2\,(t) \rightarrow 3\beta\text{-}Ca_3(PO_4)_2 + \text{CaO-doped Y-}ZrO_2\,(c)/\text{Y-doped}\,CaZrO_3 + H_2O$$

No free Y_2O_3 was observed. Thus, a homogenous solid solution of Y_2O_3 in ZrO_2 was formed and the crystal structure was of the tetragonal, cubic, or tetragonal-zirconia dual phases.

Investigation of the HA–YSZ composite patterns at 1050 °C (Fig. 4) revealed that the decomposition of HA was accelerated. TCP and $CaZrO_3$ peaks are observed and are obviously sharper than those formed at lower temperatures. Thus, based on these results, a temperature of 950 °C was chosen as the calcination temperature for HA–YSZ composite powder.

The grain sizes obtained for the composite nanopowders are presented in Table 1. The samples calcined at 850 °C exhibit small grains for hydroxyapatite and zirconia phases, while the samples calcined at 950 °C and 1050 °C demonstrate larger grains. Thus, increasing the calcination temperature might assist grain growth although all the composite powders are comprised of nanograins. By manipulating the grain growth kinetics, it is possible to adjust the microstructure of the HA–YSZ composite nanopowders. The transformation from the high temperature phases of tetragonal and cubic ZrO_2 to the monoclinic phase in the stabilized ZrO_2 is prevented. With the addition of Y_2O_3, the chemical free energy of each polymorph of zirconia changes such that the tetragonal and/or cubic phases can be stabilized at room temperature [26,7]. Moreover, because of the lower surface energy of the tetragonal phase (γ_t = 0.77 J/m^2) [27] compared to that of the monoclinic phase (γ_m = 1.13 J/m^2), a surface energy effect obtains which is related to the stability of the phase in pure and stabilized zirconia [26].

Grain boundary diffusion is generally claimed to be involved in grain growth in nanostructured materials [32]. Some factors such as grain boundary segregation [33], solute drag [34], and second phase (Zener) drag [35] have been explained to influence the grain-boundary mobility in nanostructured materials that may, in turn, strongly affect the kinetics of the grain growth involved [32]. In yttria-stabilized zirconia, crystal

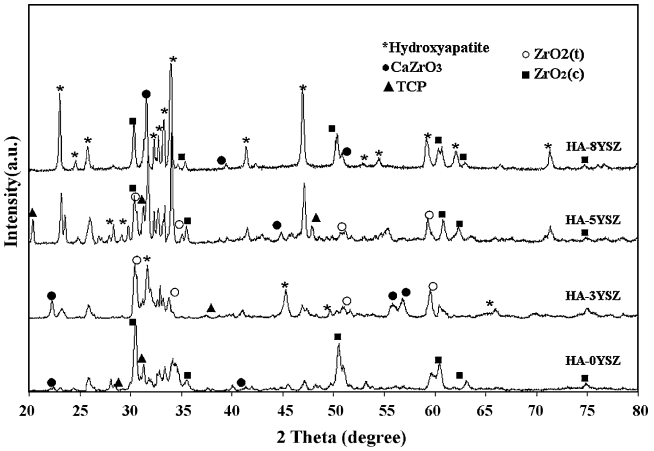

Fig. 4. XRD patterns of composite nanopowders obtained with various amounts of Y_2O_3 after calcination at temperature of 1050 °C for 1 h.

Table 2
Lattice parameters (a and c) of the HA in HA–YSZ composite powders and HA unit cell volume.

Samples	Lattice parameters of HA		HA volume (Å^3)
	a (Å)	c (Å)	
HA	9.42	6.88	1581.4
HA–0YSZ	9.47	6.84	1589.3
HA–3YSZ	9.47	6.84	1588.7
HA–5YSZ	9.45	6.85	1583.7
HA–8YSZ	9.48	6.85	1595.3

Table 3
Lattice parameters (a and c) of zirconia in HA–YSZ composite powders.

Samples	Lattice parameters of zirconia	
	a (Å)	c (Å)
ZrO_2 (t)	5.119	5.1418
ZrO_2 (c)	5.074	–
HA–0YSZ	5.112	–
HA–3YSZ	5.127	5.0738
HA–5YSZ	5.123	5.0568
HA–8YSZ	5.089	–

growth is hindered and phase transition is delayed since the mass transport by surface diffusion is lower than that for pure zirconia [7,26]. According to Matsui's work [35], during calcination, grain growth behavior can be reasonably explained by the solute-drag mechanism of Y^{3+} ions segregating along the grain boundary. The driving force of the grain boundary is closely related to the segregation of Y^{3+} ions, which directly affects grain growth [7,26,35]. In this case, the lower grain-boundary mobility or lower grain growth was assumed to be due to solute segregation at the grain boundary [7,26,35]. The enhanced stability, as observed in the HA–YSZ composite nanopowders, can be accordingly attributed in part to their suppressed grain growth and growth rate affected by increasing Y_2O_3 content. As can be seen in the results for grain size (Table 1), the presence of zirconia inhibited the grain growth of HA particles. Thus, the composite powders containing ZrO_2 nanoparticles should be produced for the improvement of strength upon further consolidation [36].

According to Table 1, increasing calcination temperatures increased HA crystallinity, but ZrO^{2+} substitution in the HA lattice resulted in reduced HA crystallinity in the presence of ZrO_2 particles.

Table 2 presents the lattice parameters and the volume of HA unit cell into the composites, as calculated from the angles of X-ray diffraction peaks ((0 0 2) and (0 0 3)). As shown in this table, the volume of HA unit cell increased in all the samples. These increases in volume resulted mainly from increases in the (a) parameters, rather than from the (c) values. The increased tendency of HA decomposition due to reaction with ZrO_2 can be explained as resulting from the removal of calcium from HA and its dissolution into zirconia. It is suggested that the removal of calcium ions from HA involves an ion exchange reaction with ZrO^{2+} ions from the ZrO_2 [20]. The radius of a ZrO^{2+} ion is about 0.21 nm; that of calcium is about 0.1 nm [20]. Thus, when the ZrO^{2+} ion is substituted for Ca^{2+}, the volume of HA unit cell increases. This exchange, therefore, explains the increased volume of the HA unit cell as shown in Table 2. Evis [20] also obtained the similar results. The exchange of Ca^{2+} and ZrO^{2+} ions happen with minimum rearrangement in HA and zirconia structures, where the surfaces of ZrO_2 and HA are in contact. For example, in the HA structure, the exchange of ZrO^{2+} ions for Ca^{2+} ions explains the increased tendency for decomposition. The large ZrO^{2+} ion introduces strain into the HA structure, accelerating the HA decomposition process [11,20]. This solid solution of calcium into ZrO_2 leads to its transformation to cubic and tetragonal phases, as already explained. Solid solution formation and the lattice parameter change in ZrO_2 were investigated using XRD data and presented in Table 3. Substitution of Zr^{4+} by Ca^{2+} results in the (a) parameter of the ZrO_2 crystal to increase; this is because of the ionic size of Ca^{2+} is 0.1 nm and that of Zr^{4+} is 0.072 nm [11]. Calcium ions are larger than Zr^{4+} ions; thus, they cannot enter the interstitial sites in ZrO_2 crystals. Rather, they can substitute Zr^{4+} sites, which results in a substantial increase in the (a) lattice parameter value of t-ZrO_2 and c-ZrO_2.

3.4. XRF analysis

The amounts of yttria in the composites obtained after calcination of composite dried gels at a temperature of 950 °C for 1 h were confirmed by X-ray fluorescence spectroscopy as reported in Table 4. LOI (Lost on Ignition) was calculated by means of weight loss of TG curves (Fig. 1(a–d)). Pure HA has a theoretical composition of: Ca/P wt ratio, 2.157 [3]. According to Table 4, Ca/P wt ratios of all the composite powders had values slightly smaller than those of the stoichiometric HA. Some calcium deficiency of HA is attributed to the presence of ZrO_2 and the pH value of the primary sol. After preparation of the HA–YSZ sol, a pH level of 1.05 was detected; so one possibility is that the high acidity of the sol solution favors a more acidic formation of calcium phosphate, having a lower

Table 4
Chemical compositions of the HA–YSZ composite powders.

Samples	wt% CaO	wt% P_2O_5	wt% Ca/P	wt% ZrO_2	wt% Y_2O_3	LOI%
HA–0YSZ	22.44	17.99	2.05	15.03	0	45
HA–3YSZ	23.50	18.11	2.11	15.40	1.71	44
HA–5YSZ	28.09	21.72	2.12	15.61	2.85	35
HA–8YSZ	26.28	19.05	2.27	15.01	4.56	40

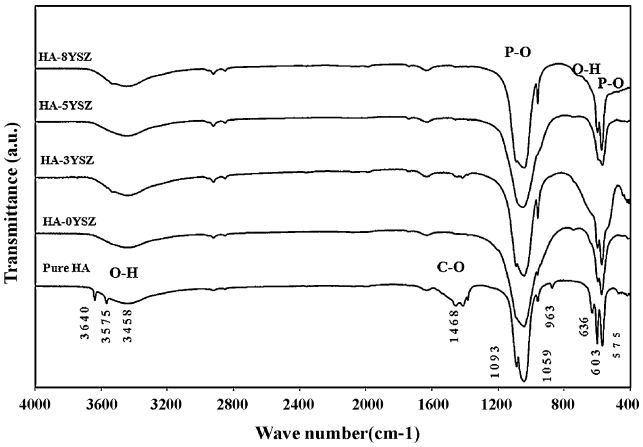

Fig. 5. FTIR spectra of the synthesized composite nanopowders with various amounts of Y_2O_3 after calcination at temperature of 950 °C for 1 h.

Ca/P wt ratio than the stoichiometric HA [14,37]. In addition, the reactions between HA and ZrO_2, explained above, cause the calcium deficiency.

3.5. FTIR analysis

As shown in the FTIR spectra (Fig. 5), the two bands at 636, 3575 and 3640 cm^{-1} belong to hydroxyl vibration. These spectra indicate the formation of a HA structure containing sharp O–H and P–O bands. The bands at 603 and 575 cm^{-1} are the typical bands of phosphate bending vibration, while the bands at 1059, 1093, and 963 cm^{-1} are due to phosphate stretching vibration [13,14,37]. Carbonate type B presents characteristic bands in the region 1500–1400 cm^{-1} [14,37]. The appearance of CO_3^{2-} functional group at 1468 cm^{-1} is related to the carbonate group and suggests that carbon from the organics does not pyrolyze completely and may, instead, dissolve into the HA structure. In addition, the carbonate apatite can originate due to the presence of CO_2 from air or due to the liberation of alkyl groups (which are by-products). This peak makes HA more similar to the composition of natural bone and, then, forms ostoid HA so as to improve osteogenesis [38]. Carbonated apatite powders can reveal in vitro resorption rates similar to the resorption rates of natural bone minerals which are higher than that of pure HA [39].

FTIR analysis of HA–YSZ composite powders indicates that, rather than the absorbance band at 3458 cm^{-1}, the O–H absorbance band of 3575 and 3640 cm^{-1} disappears, which is typical for absorbed water (H_2O); this is while the phosphate stretching region is broader. The effect of zirconia on the hydroxyl ions associated with the stretching mode at 3458 cm^{-1} tends to intensify this absorption band. As the FTIR spectra did not show absorption bands related to zirconia, it is possible that the disappearance or masking of the O–H stretching mode was caused by the existence of calcia stabilized zirconia and ZrO_2, as reported by XRD patterns [40]. The vibrational bands of the phosphate ions are observed in all the composite nanopowders. In pure HA, the PO_4^{3-} band is well shown at 603 and 575 cm^{-1}, but the resolution drops in the composite sample with decreasing peak area. The band around 1059 cm^{-1} appears in pure HA with peaks well resolved at 1093 and 1059 cm^{-1}, but the resolution decreases and broadening takes place in the case of composite powders [36,41].

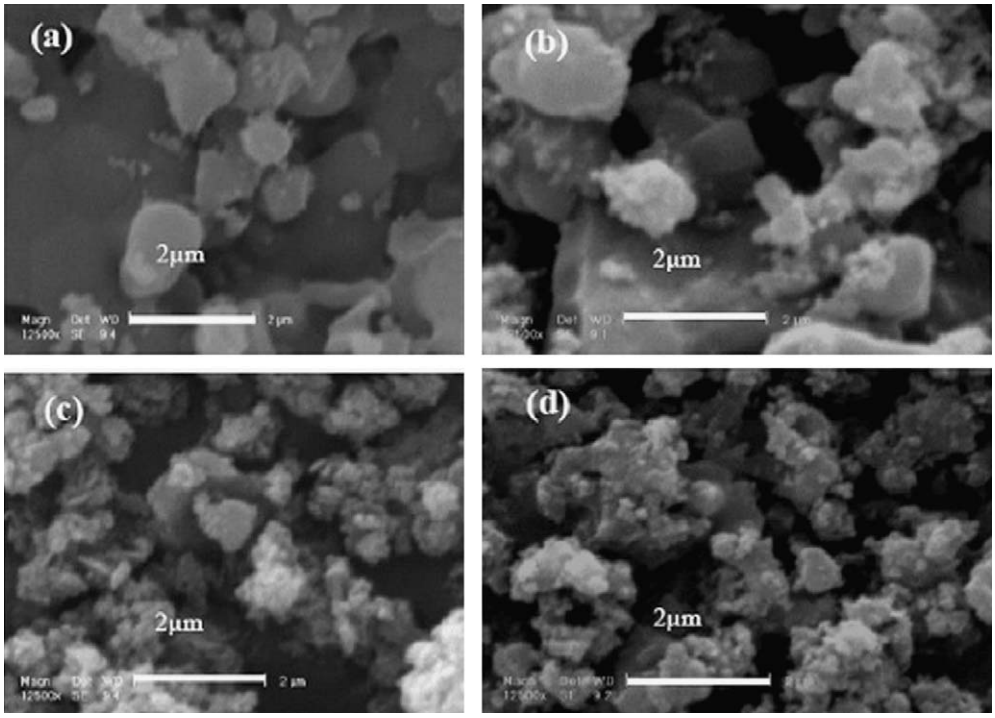

Fig. 6. SEM micrographs of HA–YSZ composite nanopowders with various amounts of Y_2O_3 showing the morphology and particle size distribution of the powders: (a) HA–0YSZ, (b) HA–3YSZ, (c) HA–5YSZ, and (d) HA–8YSZ.

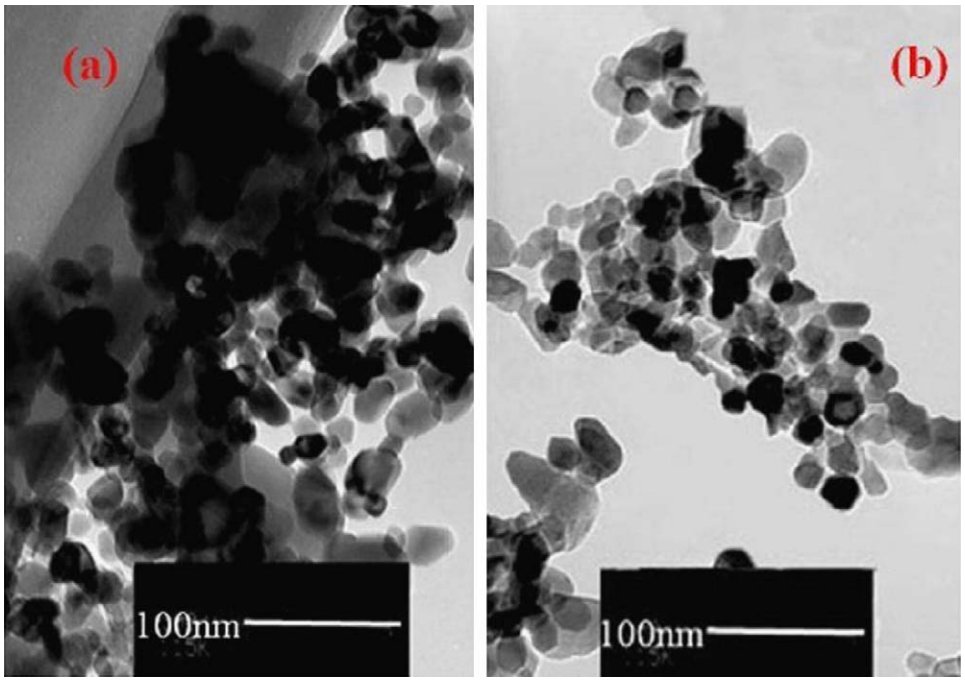

Fig. 7. TEM micrographs of (a) HA–8YSZ and (b) HA–3YSZ composites nanopowders calcined at 950 °C for 1 h. The nanoparticles size distribution and morphology of the composites obtained from the sol–gel method can be observed.

3.6. SEM evaluation

Fig. 6 shows the morphology and particle size distribution of the HA–YSZ composite nanopowders. The composite powders appear to be composed of spherical and very fine particles that aggregate to form agglomerates. The mean aggregating size of the calcined particles was approximately 500 nm–8 μm. The larger HA particles are covered by smaller particles, which are less than 500 nm. Powder porosity is believed to result from the liberation of volatile components such as NO_2 (from nitrate) and CO_2 (from carbonate or alkyl groups) at calcined temperatures.

3.7. TEM analysis

Fig. 7 shows the bright field TEM photographs of (a) HA–8YSZ and (b) HA–3YSZ powders (as samples). The ZrO_2 particles are mostly spherical in shape while the lighter ones are HA. The YSZ particles were uniformly embedded between the HA particles. It can also be seen in the micrographs that ZrO_2 particles (20–30 nm) are uniformly distributed in the HA matrix, which is close to the crystal sizes determined by the XRD patterns and Scherer's equation (Table 1). The uniform distribution of zirconia nanopowders in the HA matrix of the composite would be highly beneficial for obtaining homogeneous powders [11,41,42]. It can be seen that the average size of HA grains in the HA–YSZ composite powders are 40–80 nm, indicating the function of YSZ particles as an HA grain growth inhibitor during calcination. The morphology and the uniform distribution of ZrO_2 nanoparticles have also been reported in other studies [41,42].

Over the past few decades, a variety of graft materials have been used as substitutes for hard tissues. Ceramics are regarded as attractive materials for joints or joint surface materials. Due to their ease of processing and formation and their superior mechanical properties, a number of ceramic materials have been investigated as bone substitute materials [43,44]. The development of bioceramics results in replacing parts of the skeletal system. Thus, it is important to develop new types of bioceramics [43,44].

Since nanostructured materials have higher amounts of particle boundaries compared to the micron particle size materials, more sites are present for osteoblast adhesion on the nanostructured compared to microstructured materials [44]. The results of the present work open up new possibilities for producing bioactive HA–YSZ composite nanopowders with a verity of mechanical properties that meet the requirements of various biological load-bearing applications. Reports on the biological reactivity of the HA–YSZ composites suggest that these biomaterials present potentials for future biomedical applications [45].

4. Conclusions

Homogeneous composite nanopowders of hydroxyapatite/30 wt% yttria-stabilized zirconia (HA–YSZ) containing 0, 3, 5, and 8 mol% Y_2O_3 were synthesized with optimum amount of chemical precursors and adjusting sol–gel method parameters. Calcination temperature at 950 °C was chosen because the composite powders calcined at this temperature exhibited suitable crystallinity and phase properties. All the powders studied consisted of big agglomerates composed of nanoparticles. HA–YSZ composite nanopowders of ∼40–80 nm in size containing various amounts of Y_2O_3 were prepared. ZrO_2 of a spherical shape was formed which ranged in size from 20 to

30 nm. By this process, the HA–YSZ composite nanopowders needed for various biomedical applications were successfully synthesized.

Acknowledgements

The authors are grateful for support of this research by Isfahan University of Technology.

References

[1] Z.C. Wang, C.J. Lin, F. Chen, Preparation and characterization of nano-sized hydroxyapatite particles and hydroxyapatite/chitosan nanocomposite for use in biomedical materials, Mater. Lett. 57 (2002) 858–861.
[2] M. Mazaheri, M. Haghighatzadeh, A.M. Zahedi, S.K. Sadrnezhaad, Effect of a novel sintering process on mechanical properties of hydroxyapatite ceramics, J. Alloys Compd. 471 (2009) 180–184.
[3] P. Ducheyne, M. Marcolongo, E. Schepers, in: L.L. Hench, J. Wilson (Eds.), An Introduction to Bioceramic, World Scientific Publishing Co., Singapore, 1993, pp. 281–297.
[4] I. Mobasherpour, M. Solati Hashjin, S.S. Razavi Toosi, R. Darvishi Kamachali, Effect of the addition ZrO_2–Al_2O_3 on nanocrystalline hydroxyapatite bending strength and fracture toughness, Ceram. Int. 35 (2009) 1569–1574.
[5] X. Miao, Y. Chen, H. Guo, K.A. Khor, Spark plasma sintered hydroxyapatite–yttria stabilized zirconia composites, Ceram. Int. 30 (2004) 1793–1796.
[6] C. Piconi, G. Maccauro, Zirconia as a ceramic biomaterial, Biomaterials 20 (1999) 1–25.
[7] C.W. Kuo, Y.H. Lee, I.M. Hung, M.C. Wang, S.B. Wen, Crystallization kinetics and growth mechanism of 8 mol% yttria-stabilized zirconia (8YSZ) nano-powders prepared by a sol–gel process, J. Alloys Compd. 453 (2008) 470–475.
[8] E. Adolfsson, Z. Shen, Densification of zirconia–hydroxyapatite ceramics without phase changes, Key Eng. Mater. 309–311 (2006) 1141–1144.
[9] S.A. Catledge, M.D. Fries, Y.K. Vohra, W.R. Lacefield, J.E. Lemons, S. Woodard, R. Venugopalan, Nanostructured ceramics for biomedical implants, J. Nanosci. Nanotechnol. 2 (2002) 293–312.
[10] T.J. Webster, C. Ergun, R.H. Doremus, R.W. Siegel, R. Bizios, Enhanced functions of osteoblasts on nanophase ceramics, Biomaterials 21 (2000) 1803–1810.
[11] Y.M. Sung, Y.K. Shin, J.J. Ryu, Preparation of hydroxyapatite/zirconia bioceramic nanocomposites for orthopedic and dental prosthesis application, Nanotechnology 18 (2007) 065602.
[12] C.Y. Chiu, H.C. Hsu, W.H. Tuan, Effect of zirconia addition on the microstructural evolution of porous hydroxyapatite, Ceram. Int. 33 (2007) 715–718.
[13] W. Feng, L.M. Sena, L.Y. Penga, Q.B.D.Y. Xin, A simple sol–gel technique for preparing hydroxyapatite nanopowders, Mater. Lett. 59 (2005) 916–919.
[14] D.M. Liu, Q. Yang, T. Troczynski, W.J. Tseng, Effect of hydrolysis on the phase evolution of water-based sol–gel hydroxyapatite and its application to bioactive coatings, J. Mater. Sci.: Mater. Med. 13 (2002) 657–665.
[15] JCPDS Card No. 9-432, 1994.
[16] JCPDS Card No. 27-0997, 1994.
[17] JCPDS Card No. 17-0923, 1994.
[18] B.D. Cullity, Elements of X-ray Diffraction, Addison-Wesley, 1978.
[19] Y.X. Pang, X. Bao, Influence of temperature, ripening time and calcination on the morphology and crystallinity of hydroxyapatite nanoparticles, J. Eur. Ceram. Soc. 23 (2003) 1697–1704.
[20] Z. Evis, Reactions in hydroxyapatite–zirconia composites, Ceram. Int. 33 (2007) 987–991.
[21] X. Changrong, C. Huagiang, W. Hong, Y. Pinghua, Sol–gel synthesis of yttria stabilized zirconia membranes through controlled hydrolysis of zirconium alkoxide, Membr. Sci. 162 (1999) 181–188.
[22] H. Dislich, in: L.C. Klein (Ed.), Sol Gel Technology for Thin Films, Fibers, Performs, Electronics and Specialty Shapes, Noyes Publications, Park Ridge, New Jersey, 1988, p. 50.
[23] S.C. Cameron, A.G. Karlis, B.N. Besim, Critical ageing of hydroxyapatite sol–gel solutions, Biomaterials 19 (1998) 2291–2296.
[24] I. Bogdanoviciene, A. Beganskiene, T. Kaia, Calcium hydroxyapatite, $Ca_{10}(PO_4)_6(OH)_2$ ceramics prepared by aqueous sol–gel processing, Mater. Res. Bull. 41 (2006) 1754–1762.
[25] A. Balamurugan, S. Kannan, S. Rajeswari, Structural and electrochemical behavior of sol–gel zirconia films on 316L stainless-steel in simulated body fluid environment, Mater. Lett. 57 (2003) 4202–4205.
[26] C.W. Kuo, Y.H. Lee, K.Z. Fung, M.C. Wang, Effect of Y_2O_3 addition on the phase transition and growth of YSZ nanocrystallites prepared by a sol–gel process, J. Non-Cryst. Solids 351 (2005) 304–311.
[27] Y.T. Zhao, Z. Zhang, Q.X. Dai, D.Y. Lin, S.M. Li, Microstructure and bond strength of HA (ZrO_2 + Y_2O_3)/Ti6Al4V composite coatings fabricated by RF magnetron sputtering, Surf. Coat. Technol. 200 (2006) 5354–5363.
[28] H. Guo, K.A. Khor, Y.C. Boey, X. Miao, Laminated and functionally graded hydroxyapatite/yttria stabilized tetragonal zirconia composites fabricated by spark plasma sintering, Biomaterials 24 (2003) 667–675.
[29] R. Ramachandra, T.S. Kannan, Synthesis and sintering of hydroxyapatite–zirconia composites, Mater. Sci. Eng. C 20 (2002) 187–193.
[30] R.B. Heimann, T.A. Vu, Effect of CaO on thermal decomposition during sintering of composite hydroxyapatite–zirconia mixtures for monolithic bioceramic implants, J. Mater. Sci. Lett. 16 (1997) 437–439.
[31] Z. Evis, C. Ergun, R.H. Doremus, Hydroxyapatite–zirconia composites: thermal stability of phases and sinter ability as related to the CaO–ZrO_2 phase diagram, J. Mater. Sci. 40 (2005) 1127–1134.
[32] N. Hosseini, M.H. Abbasi, F. Karimzadeh, M.H. Enayati, Structural evolution and grain growth kinetics during isothermal heat treatment of nanostructured Al 6061, Mater. Sci. Eng. A 525 (2009) 107–111.
[33] J. Weissmüller, Alloy effects in nanostructures, Nanostruct. Mater. 3 (1993) 261–272.
[34] A. Michels, C.E. Krill, H. Ehrhardt, R. Birringer, D.T. Wu, Modeling the influence of grain-size-dependent solute drag on the kinetics of grain growth in nanocrystalline materials, Acta Mater. 47 (1999) 2143–2152.
[35] K. Matsui, H. Yoshida, Y. Ikuhara, Grain boundary structure and microstructure development mechanism in 2–8 mol% yttria-stabilized zirconia polycrystals, Acta Mater. 56 (2008) 1315–1325.
[36] R. Kumar, P. Cheanga, K.A. Khor, Radio frequency (RF) suspension plasma sprayed ultra-fine hydroxyapatite (HA)/zirconia composite powders, Biomaterials 24 (2003) 2611–2621.
[37] M.H. Fathi, A. Hanifi, V. Mortazavi, Preparation and bioactivity evaluation of bone-like hydroxyapatite nanopowder, J. Mater. Process. Technol. 202 (2008) 536–542.
[38] L.S. Wojciech, P. Shuk, K. Byrappa, E.R. Riman, Mechanochemical–hydrothermal synthesis of carbonated apatite powders at room temperature, Biomaterials 23 (2002) 699–710.
[39] Y. Doi, T. Shibutani, Y. Moriwaki, T. Kajimoto, Y. Iwayama, Sintered carbonate apatites as bioresorbable bone substitutes, J. Biomed. Mater. Res. 39 (1998) 603–610.
[40] V.V. Silva, F.S. Lameiras, Synthesis and characterization of composite powders of partially stabilized zirconia and hydroxyapatite, Mater. Charact. 45 (2000) 51–59.
[41] X.F. Xiao, R.F. Liu, Y.Z. Zheng, Hydrothermal-electrochemical codeposited hydroxyapatite/yttria stabilized zirconia composite coating, J. Mater. Sci. 41 (2006) 3417–3424.
[42] Y. Nayak, R.P. Rana, S.K. Pratihar, S. Bhattacharyya, Pressureless sintering of dense hydroxyapatite–zirconia composites, J. Mater. Sci.: Mater. Med. 19 (2008) 2437–2444.
[43] M.H. Fathi, M. Kharaziha, Two-step sintering of dense, nanostructural forsterite, Mater. Lett. 63 (2009) 1455–1458.
[44] R. Narayanan, T.Y. Kwon, K.H. Kim, Direct nanocrystalline hydroxyapatite formation on titanium from ultrasonated electrochemical bath at physiological pH, Mater. Sci. Eng. C 28 (2008) 1265–1270.
[45] V.V. Silva, F.S. Lameiras, Z.I.P. Lobato, Biological reactivity of zirconia–hydroxyapatite composites, J. Biomed. Mater. Res.: Appl. Biomater. 63 (2002) 583–590.